Identification and characterization of a unique cysteine residue proximal to the catalytic site of *Arabidopsis thaliana* carotenoid cleavage enzyme 1

Shukui Guo, Jason Boyd, Ramaswami Sammynaiken, and Michèle C. Loewen

Abstract: AtCCD1 and AtNCED3 are related carotenoid cleavage enzymes from *Arabidopsis thaliana* that catalyze the oxidative cleavage of, respectively, the 9,10 (9′,10′) double bonds of carotenoid substrates such as β-carotene, and the 11,12 double bond of 9-*cis* epoxycarotenoids. Although the cellular and cleavage functionalities of these enzymes have been reported, their mechanisms and related structural environments mediating these disparate specificities in homologous enzymes have not been well characterized. By relating the differences observed in UV and visible light absorption and Cu(II) electron paramagnetic signals to variations in sequence alignments and 3-D homology models of the two *A. thaliana* enzymes, we identified a putatively proximal cysteine residue (Cys352) in AtCCD1 that is not conserved in AtNCED3. Spectral analysis of the Cys to Ala mutant confirmed its uniqueness and proximity to the metal binding site, but precluded any role for the residue in the mediation of the observed metal binding affinity or associated steric constraint differences. Further analysis of kinetic substrate cleavage properties indicated a decrease in V_{max} and a subtle increase in K_m for the C352A mutant compared with those observed for the wild-type, thus confirming catalytic site proximity and suggesting possible roles for the unique cysteine in the modulation of substrate affinity and (or) the reaction rate of AtCCD1.

Key words: carotenoid cleavage enzymes, carotenoids, type II Cu center, cysteine mutagenesis.

Résumé : AtCCD1 et AtNCED3 sont des enzymes de clivage des caroténoïdes apparentées chez *Arabidopsis thaliana* qui catalysent respectivement le clivage de la double liaison 9,10 (9′,10′) de substrats caroténoïdes comme la ß-carotène et la double liaison 11,12 des 9-*cis* époxycaroténoïdes. Alors que les fonctionnalités cellulaires et de clivage de ces enzymes ont été rapportées, les mécanismes enzymatiques et les environnements structurels responsables des spécificités disparates de ces enzymes homologues ne sont pas bien caractérisés. En reliant les différences observées par absorption UV/visible et les signaux électroniques paramagnétiques du Cu(II) avec les alignements de séquence et les modèles d'homologies tridimensionnelles des deux enzymes de *A. thaliana*, nous avons identifié un résidu cystéine vraisemblablement proximal (Cys352) chez AtCCD1 qui n'est pas conservé chez ArNCED3. L'analyse spectrale de mutants Cys/Ala ont confirmé son caractère unique et sa proximité du site de liaison métallique, mais exclut tout rôle comme médiateur de l'affinité de liaison au métal observée ou dans les différences de contraintes stériques associées. Des analyses plus poussées de la cinétique de clivage des substrats ont révélé une diminution du V_{max} et une faible augmentation du K_m chez le mutant C352A comparativement au type sauvage, confirmant sa proximité du site catalytique et suggérant des rôles possibles de cette cystéine unique dans la modulation de l'affinité du substrat et/ou du taux de réaction de AtCCD1.

Mots-clés : enzymes de clivage des caroténoïdes, caroténoïdes, centre Cu de type II, mutagenèse de la cystéine.

[Traduit par la Rédaction]

Received 14 November 2007. Revision received 8 February 2008. Accepted 3 March 2008. Published on the NRC Research Press Web site at bcb.nrc.ca on 22 May 2008.

S. Guo and J. Boyd. Plant Biotechnology Institute, National Research Council Canada, 110 Gymnasium Place, Saskatoon, SK S7N 0W9, Canada.
R. Sammynaiken. SK Structural Science Centre, University of Saskatchewan, 110 Science Place, Saskatoon, SK S7N 5C9, Canada; Department of Biochemistry, University of Saskatchewan, 107 Wiggins Road, Saskatoon, SK S7N 5E5, Canada.
M.C. Loewen.[1] Plant Biotechnology Institute, National Research Council Canada, 110 Gymnasium Place, Saskatoon, SK S7N 0W9, Canada; Department of Biochemistry, University of Saskatchewan, 107 Wiggins Road, Saskatoon, SK S7N 5E5, Canada.

[1]Corresponding author (e-mail: michele.loewen@nrc.ca).

Introduction

Carotenoid cleavage enzymes catalyze the oxidative cleavage of double bonds of carotenoid substrates, yielding physiologically important signaling molecules (Tan et al. 2003; Bouvier et al. 2005). These enzymes are part of an increasingly recognized family, with representatives now identified in organisms ranging from bacteria to plants and humans (Moise et al. 2005; Auldridge et al. 2006). Significant variability exists between homologous family members in terms of substrate affinities, cleavage specificities, and associated reaction rates. Two of the best characterized carotenoid cleavage enzymes include the *Arabidopsis thaliana* carotenoid cleavage dioxygenase 1 (AtCCD1) and the *A. thaliana* 9-*cis* epoxycarotenoid cleavage dioxygenase 3 (AtNCED3). AtCCD1 is localized to the cytosolic fraction of leaf cells and cleaves the 9,10 and 9′,10′ double bonds of

 doi:10.1139/O08-031

Fig. 1. Carotenoid cleavage reactions mediated by AtCCD1 (A) and AtNCED3 (B).

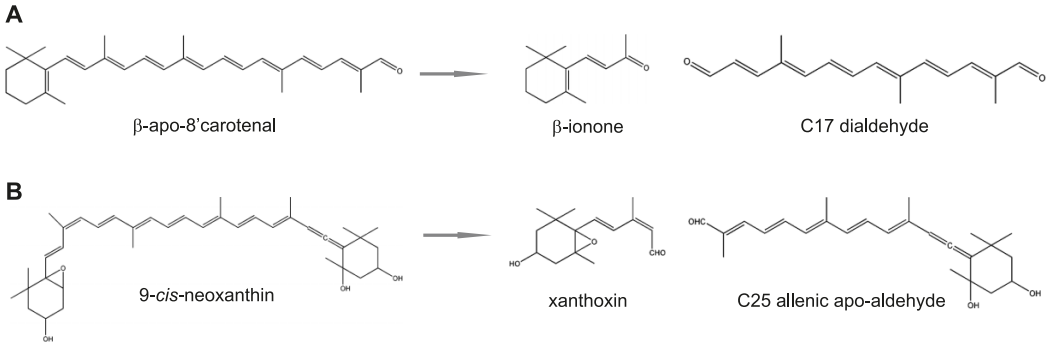

a variety of carotenoid substrates, including β-carotene, lutein, and β-apo-8′-carotenal, yielding compounds related to β-ionone and dialdehyde fragments (Fig. 1A) (Schwartz et al. 2001; Schmidt et al. 2006). In contrast, AtNCED3 is localized to the plastid and cleaves the 11,12 double bond of 9-*cis* epoxycarotenoids (violaxanthin and neoxanthin), producing C25 aldehyde compounds and the important abscisic acid hormone precursor molecule, xanthoxin (Fig. 1B) (Iuchi et al. 2001). AtNCED3 maintains high homology with, and a similar function to, the maize VP14 and cowpea NCED3 enzymes known to be responsible for drought stress inducible abscisic acid biosynthesis (Schwartz et al. 1997; Iuchi et al. 2001). AtCCD1 and AtNCED3 share approximately 38% amino acid sequence identity.

Carotenoid cleavage enzymes are non-heme ferrous ion-dependent oxygenases (Ryle and Hausinger 2002). Non-heme ferrous enzymes lack intense porphyrin-based electronic transitions, and the ferrous centers are often spectroscopically silent (Solomon 2001), making analysis of the active site mechanisms by classical biophysical methods more challenging. However, the crystal structure of a related cyanobacterial apo-carotenal oxygenase (ACO) was recently reported (Kloer et al. 2005). In this crystal structure, the non-heme Fe^{2+} is coordinated by the $^{\varepsilon}N$ atoms of four conserved histidine residues, differing somewhat from the 2-His-1-carboxylate facial triad structure identified in other mononuclear non-heme Fe(II) enzymes (Hegg and Que 1997). Site-directed mutagenesis of a mammalian carotenoid cleavage enzyme has further confirmed the importance of the four conserved histidines in enzyme function (Poliakov et al. 2005). In addition to providing some mechanistic insight into ACO, the crystal structure also yields a template with which other carotenoid cleavage enzyme structures can be simulated by homology modeling. Generated models can be tested by other biophysical methods, such as ultraviolet/visible (UV/Vis) absorption spectroscopy, which has been used successfully to investigate structure–function relationships in other non-heme iron enzymes (Coufal et al. 1999; Hegg et al. 1999; Franco et al. 2001; Hinks et al. 2002; Mathe et al. 2002; Kimura et al. 2005). Additionally, although low-spin ferrous is diamagnetic and thus, electron paramagnetic resonance (EPR) silent (Solomon 2001), and high-spin ferrous can only be observed in parallel mode EPR (Hinks et al. 2002), EPR spectra revealing important structural information for non-heme iron proteins have been reported under oxidizing conditions (Deligiannakis et al. 1997; Hinks et al. 2002; Mathe et al. 2002; Rocklin et al. 2004), labeled with NO (Deligiannakis et al. 1997; Coufal et al. 1999; Hegg et al. 1999; Rocklin et al. 1999; D'Autreaux et al. 2005), or as Cu(II)-substituted derivatives (Whiting et al. 1997; Coulter et al. 1999; Hegg et al. 1999; Hogan et al. 2000).

Although some of the basic cellular and cleavage functions of carotenoid cleavage enzymes have been reported, the enzymatic mechanisms and related structural aspects leading to the observed diversity in substrate and cleavage specificities and catalytic reaction rates associated with the different members of this family remain largely uncharacterized. To understand these structure–function relationships, we initiated comparative UV/Vis absorption analyses of the catalytic metal binding sites of recombinant forms of AtCCD1 and AtNCED3, which indicated differences related to either affinity or steric accessibility of the iron sites. Further, relating differences in observed Cu(II) EPR signals to amino acid sequence alignments and 3-D homology models led to the identification of a cysteine residue (Cys352) proximal to the catalytic site in AtCCD1 that is not conserved in AtNCED3. Spectral characterization of the AtCCD1 C352A mutant confirmed the residue's proximal localization to the metal binding site, but negated a role in mediating the metal affinity- and (or) accessibility-related differences. Subsequent kinetic analyses yielded evidence that further supported the proximal catalytic site localization of the residue and suggested a possible role for the unique cysteine in the mediation of substrate binding and (or) cleavage reaction of this enzyme.

Materials and methods

Materials

All materials were obtained from Sigma–Aldrich with the following exceptions: *Escherichia coli* strain BL21(DE3) was from Novagen; pGEX2T was from GE Healthcare; pRL296a was a gift from M. Cygler, Biotechnology Research Institute (Montreal, Quebec, Canada); Quikchange Site Directed Mutagenesis kit was from Stratagene; glutathione-*S*-transferase (GST)–agarose was from Amersham Biosciences.

Overexpression and purification of recombinant enzymes

cDNAs encoding wild-type AtCCD1, AtNCED3, and the related AtCCD1 site-specific C352A mutant were overexpressed in *E. coli* strain BL21(DE3), using pGEX2T or pRL296a vectors to encode GST fusion proteins. The site-

specific mutation was introduced into the AtCCD1 cDNA using the Quickchange Site Directed Mutagenesis kit, according to the manufacturer's instructions,with the following primers: forward primer, 5′-GATGAAGTCGTCCTCATCACTGCTCGTCTTGAGAATCCAG-3′; reverse primer. 5′-CTGGATTCTCAAGACGAGCAGTGATGAGGACGACTTCATC-3′. Single colony transformants were used to inoculate 2× YT medium (16 g tryptone, 10 g yeast extract, 5 g NaCl per litre) with 50 μg/mL ampicillin, and were grown with shaking at 37 °C. Upon reaching an OD_{600} of 1.0, 0.1 mmol/L isopropyl β-D-thiogalactopyranoside was added to the cultures, which were subsequently incubated with shaking at 25 °C (AtCCD1) or 30 °C (AtNCED3) for an additional 8 h. The *E. coli* cells were harvested by centrifugation, resuspended in phosphate buffered saline (8 g NaCl, 0.2 g KCl, 1.15 g $Na_2HPO_4 \cdot 7H_2O$, and 2 g KH_2PO_4 per litre, pH 7.4) containing 1 mmol/L phenylmethanesulfonyl fluoride, and lysed with 3 × 30 s pulses of sonication. The recombinant proteins were purified with GST–agarose eluting with buffer (50 mmol/L Tris–HCl, 5 mmol/L reduced glutathione, pH 7.5) as per the manufacturer's specifications (Smith and Johnson 1988). The purity of the fusion protein was assessed by standard SDS–PAGE.

In vitro activity assays

Activity assays for AtCCD1 were performed essentially as described in Schmidt et al. (2006), with the following modifications: (*i*) 50 μL of ethanol containing different amounts of β-apo-8′-carotenal (final concentrations for kinetic experiments ranged from 0.1 to 40 μmol/L) and 20 μL of ethanolic β-octylglucoside solution (4% *w*/*v*) were combined and evaporated to dryness (*ii*) 200 μL of 100 mmol/L Bis–Tris (pH 7.0), containing 50 μg protein, 0.5 mmol/L $FeSO_4$, and 5 mmol/L ascorbate was added, and the solution was shaken vigorously and incubated at 30 °C for 15 min; (*iii*) 400 μL of methanol was subsequently added to terminate the reaction. Enzyme assay products were detected by high performance liquid chromatography analysis applied to a Supelcosil column (3.3 cm × 4.6 mm) packed with C18 reversed-phase material with a 5 μm particle size. Elution was performed with an isocratic solvent, 80% acetonitrile : 20% water (*v*/*v*), at a constant flow of 1.0 mL/min. Absorption of the eluting products was recorded at 424 nm and product identities were confirmed by UV/Vis spectral characterization based on expected absorption maxima from the literature (Wolz et al. 1999; Fester et al. 2002; Mathieu et al. 2005). The yield of C17-dialdehyde was determined by comparing the areas under the peaks with those obtained in a similar standard experiment in which the reaction time was lengthened to allow cleavage of a known quantity (5 μg) of β-apo-8′-carotenal to go to completion. Kinetic parameters were subsequently determined by standard Michaelis–Menten analyses using EnzFitter software (Biosoft).

The AtNCED3 enzymatic assay was carried out essentially as described for AtCCD1 but with the following modifications. The reaction contained 100 mmol/L Bis–Tris (pH 6.7), 5 μmol/L FeSO4, 10 mmol/L ascorbate, 0.05% Triton X-100, 1 mg/mL catalase, 40 μmol/L 9′-*cis*-neoxanthin (isolated from spinach as described previously; Britton and Young 1993), and 8 μg AtNCED3, to a total assay volume of 100 μL. The assay was incubated at 30 °C for 10 min, stopped with 50 μL of 25% Triton X-100, and extracted with 150 μL of ethyl acetate. All procedures were performed under red light to minimize photo-induced degradation to assay components and products. High performance liquid chromatography elution was initiated on the Supelcosil column conditioned with 15% acetonitrile – 85% water, with acetonitrile increasing to 35% over 10 min. Acetonitrile was subsequently increased to 65% with a step gradient followed by a linear gradient to 100% acetone over 10 min. The flow rate was maintained at 1.5 mL/min and monitored at 436 nm for the presence of the C25 allenic apo-aldehyde cleavage product. Products were identified by UV/Vis spectral characterization based on expected absorption maxima from the literature (Parry and Horgan 1991).

Fe^{2+} chelation and Cu^{2+} reconstitution of recombinant enzymes

To remove the iron from AtCCD1 or AtNCED3, the GST fusion proteins were washed with 50 mmol/L EDTA while still bound to the GST–agarose affinity resin. Residual EDTA was removed by extensively washing the resin with 30 equivalent resin volumes of PBS buffer. In cases in which metal depleted enzyme was required, the fusion protein was then immediately eluted as described above. To get Cu^{2+}-reconstituted proteins, the EDTA-treated fusion-protein loaded resin was subsequently incubated with 5 resin volumes of 200 μmol/L $CuSO_4$ with shaking for 30 min at 4 °C, washed with excess PBS buffer to remove residual free Cu^{2+}, and then also eluted as described above. Ultrafiltration (MWCO, 10 kDa) was used to concentrate the sample and replace the reduced glutathione containing elution buffer with PBS buffer.

Spectral measurements

Absorption spectra of purified fusion protein samples were measured at room temperature using a PerkinElmer Lambda 35 UV/Vis spectrophotometer. The concentrations of AtCCD1 and AtNCED3 were 6 and 11 μmol/L, respectively, in PBS buffer (as determined by measuring the absorption at 280 nm based on the relation 1 A_{280} = 0.5 mg/mL, derived from concentration estimations of protein purified from cells transformed with pGEX-1 and using bovine serum albumin as a standard (Smith and Johnson 1988)).

X-band EPR spectra were obtained at 100 K, 20 μW, and 9.3971 GHz and a modulation amplitude of 1 G using a Bruker EMX electron paramagnetic resonance spectrophotometer and an Oxford ESR 900 cryostat. Purified fusion protein or Cu^{2+} reconstituted samples (in PBS buffer) were concentrated, degassed, and sealed in EPR tubes. The protein concentrations for EPR were 0.13 and 0.11 mmol/L for AtCCD1 and AtNCED3, respectively. The EPR data were analyzed with the Bruker WINEPR program.

Homology modeling and sequence alignments

SWISS MODEL (Schwede et al. 2003) was used for comparative homology modelling by applying the ACO crystal structure as a template (Protein Data Bank accession No. 2BIW) (Kloer et al. 2005). Deep View – Swiss PDB Viewer and Visual Molecular Dynamics software were used for imaging the model (Humphrey et al. 1996; Guex and Peitsch 1997). Amino acid sequences were aligned using

Fig. 2. Purification and activity of AtCCD1 and AtNCED3 fusion proteins. (A) SDS–PAGE of purified (*i*) AtCCD1-GST and (*ii*) AtNCED3-GST fusion proteins. M, molecular mass marker. (B) Activity assay of recombinant (*i*) AtCCD1 and (*ii*) AtNCED3. HPLC profiles of reaction products. In *i*, peaks 1 and 2 represent the substrate β-apo-8′-carotenal and the C17-dialdehyde product, respectively, monitored at 424 nm. In *ii*, peaks 1 and 2 represent substrate 9′-*cis*-neoxanthin and C25 allenic apo-aldehyde product, respectively, monitored at 436 nm. Inserts show the UV/Vis absorption spectra of related peaks.

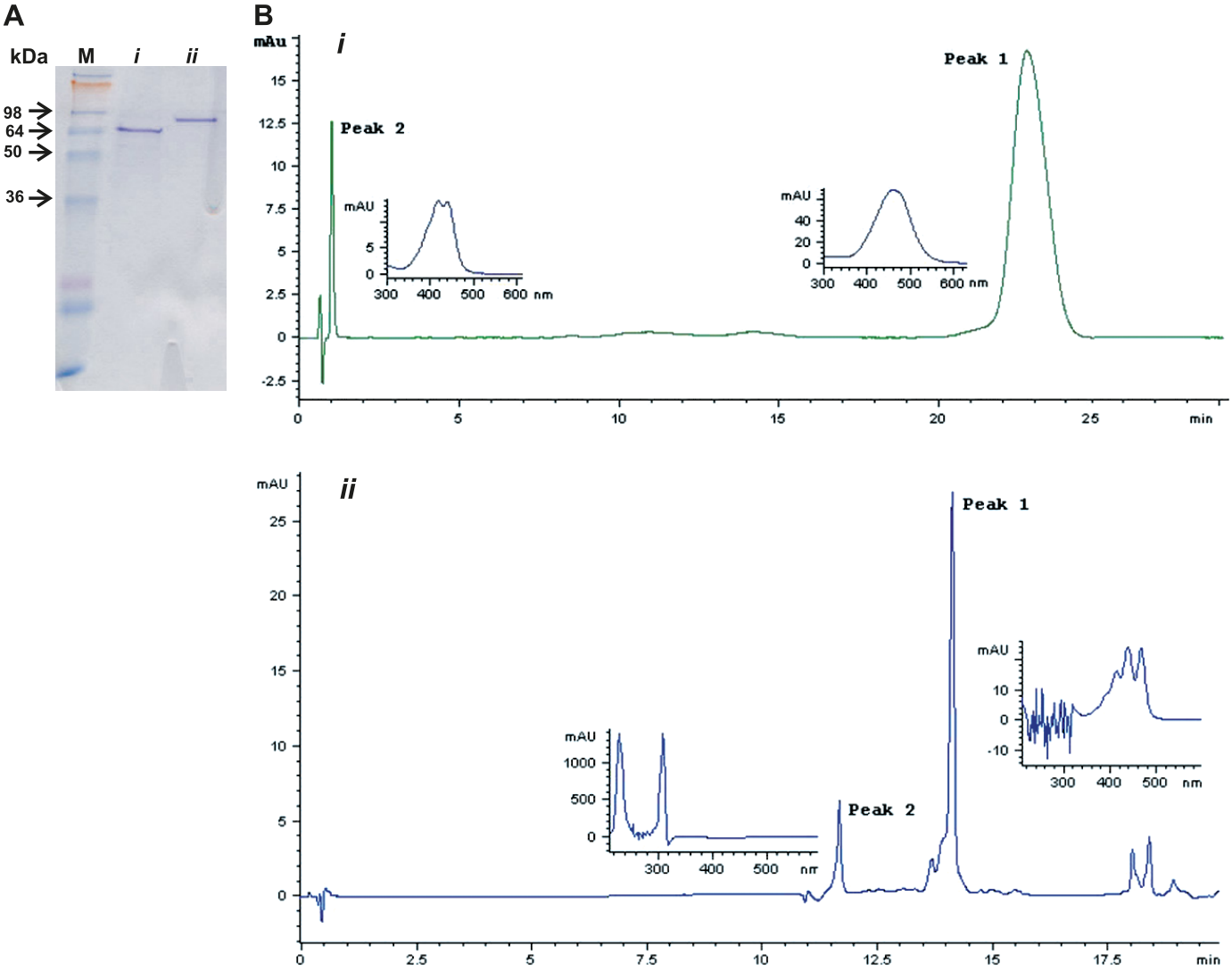

the T-Coffee multiple sequence alignment algorithm (Notredame et al. 2000). The sequence identities of ACO with AtCCD1 and AtNCED3 were determined to be 24.9% and 22.5%, respectively.

Results and discussion

Characterization of recombinant purified AtCCD1 and AtNCED3

AtCCD1 and AtNCED3 recombinant GST fusion proteins were affinity purified and characterized by SDS–PAGE analysis. Relatively pure bands were observed at the expected molecular masses of approximately 75 and 90 kDa, respectively (Fig. 2A). Average overall yields of recombinant protein were estimated at 1.5 mg of AtCCD1 and 6 mg of AtNCED3 fusion proteins purified per litre of induced *E. coli* cell culture. Non-quantitative assays probing the catalytic activity of the recombinant purified fusion proteins indicated that AtCCD1 cleaves β-apo-8′-carotenal to produce the C17-dialdehyde (Fig. 2B *i*, peak 2) as characterized by the observed absorption maxima for the product at 424 and 436 nm, which was expected, based on the literature (Wolz et al. 1999; Fester et al. 2002; Mathieu et al. 2005). Similarly, AtNCED3 cleaved 9′-*cis*-neoxanthin to produce the C25 allenic apo-aldehyde (Fig. 2B *ii*, peak 2) as confirmed by observation of the product's absorption maximum at 422 nm, which was also expected, based on the literature (Parry and Horgan 1991).

UV/Vis absorption analysis of AtCCD1 and AtNCED3 metal binding sites

UV/Vis absorption analyses of both wild-type AtCCD1 and AtNCED3 fusion proteins reveal characteristic iron absorption peaks at 413 and 650 nm, and an absorption shoulder at 530 nm (Figs. 3A and 3B, line *a*), indicating that both recombinant proteins do naturally bind iron as ex-

Fig. 3. Spectral characterization of AtNCED3 and AtCCD1 fusion proteins. (A) UV/visible light (UV/Vis) absorption spectra of AtNCED3. Line *a*, native protein; line *b*, AtNCED3 treated with 50 mmol/L EDTA; line *c*, AtNCED3 treated with 0.2 mmol/L $CuSO_4$. (B) UV/Vis absorption spectra of AtCCD1. Line 1, native protein; line 2, AtCCD1 treated with 50 mmol/L EDTA; line 3, AtCCD1 treated with 0.2 mmol/L $CuSO_4$. (C) Electron paramagnetic resonance spectrum of Cu^{2+}-reconstituted AtNCED3 acquired at 100 K, 9.3971 GHz, and 20 μW, and with a modulation of l G (1 G = 0.1 mT).

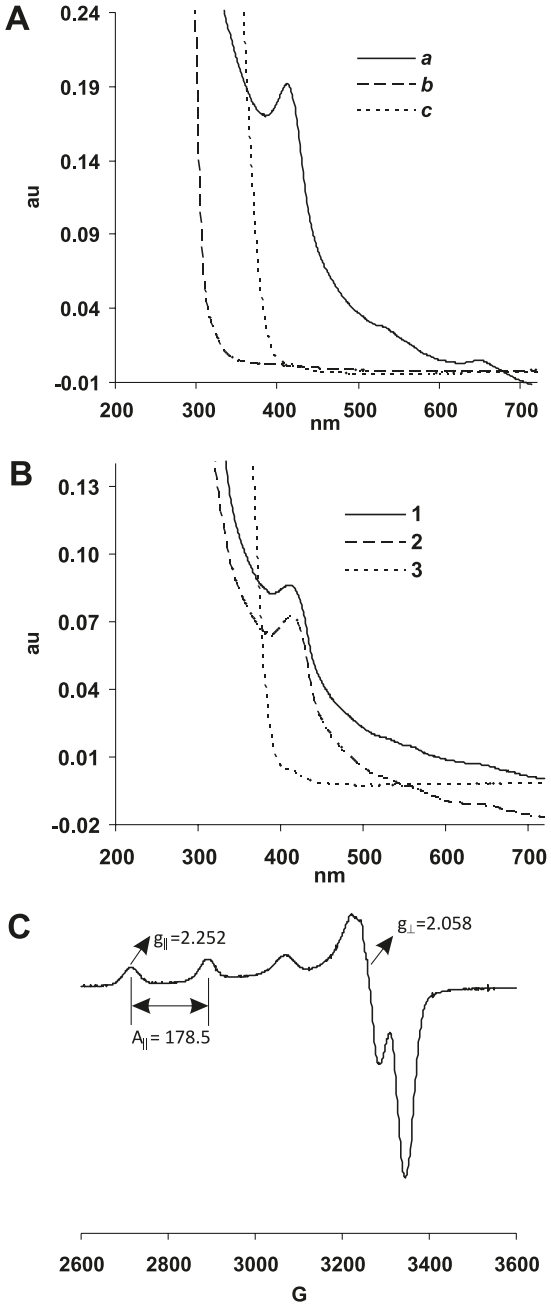

pected, based on the observed in vitro cleavage activity. Extinction co-efficients of 4550 mol/L^{-1} cm were calculated for both enzymes at 413 nm. Both chelation by EDTA and substitution by Cu^{2+} reduced the iron-specific absorption bands to below the detection limit in the case of AtNCED3 (Fig. 3A, lines *b* and *c*), indicating sequestration of iron from the enzyme. In contrast, EDTA had no effect on the AtCCD1 spectrum (Fig. 3B, line *b*), suggesting that the iron binding site in AtCCD1 is either sterically inaccessible to EDTA and (or) mediates a much stronger affinity for iron compared with the AtNCED3 enzyme. Interestingly, incubation of AtCCD1 with Cu^{2+} following EDTA treatment did lead to a loss of the absorption peaks at 413 and 650 nm (Fig. 3B, line *c*), suggesting that, although EDTA could not chelate the iron from AtCCD1, Cu^{2+} was able to displace Fe^{2+} from the binding site, most likely by substituting in its place.

EPR spectral analyses of AtNCED3 and AtCCD1 metal binding sites

To further probe the detected differences in the two metal binding sites, we initially looked for EPR signals arising from wild-type Fe^{2+}-bound AtCCD1 and AtNCED3 at l00 K, but the samples were EPR silent (data not shown). However, after Cu^{2+} substitution, AtNCED3 (Fig. 3C) yielded a type II Cu EPR signal with the following parameters: $g_{\|}$, 2.252; $A_{\|}$, 178.5 G; and $g_{\perp}$, 2.058; thus, Cu^{2+} is indeed retained in the metal binding site of the enzyme upon substitution (Kosman et al. 1998). Simulation indicates that the four expected nitrogens around the Cu^{2+} are not perfectly square planar but do correlate with the coordination observed in the ACO structure (Kloer et al. 2005). This includes coordination by the $^{\epsilon}$N, as opposed to $^{\delta}$N of histidines, as in nitrite reductase (Tocheva et al. 2004). Surprisingly, Cu^{2+}-substituted AtCCD1 showed no EPR signal (data not shown). The most obvious explanation for this result is that Cu^{2+} is not retained in the AtCCD1 active site. However, after storage of the washed reconstituted enzyme exposed to air for two months at –20 °C, a Cu(II) signal was observed by EPR (data not shown). This result, combined with the previous observation of the initial Cu^{2+}-dependent loss of the Fe^{2+} UV/Vis signal for AtCCD1, strongly suggests that a redox process is involved. Likely, the Cu^{2+} is retained in the AtCCD1 site but is reduced to the cuprous form (Cu^{+}), with corresponding oxidation of proximally located sulfhydryl groups to a disulfide form. Sulhydrl oxidation with corresponding reduction of Cu^{2+} has been well established (Creighton 1984), and if such residues were localized to the active metal binding site of AtCCD1, they could be responsible for this EPR silence.

Putative positional evaluation of cysteine residues in AtCCD1 and AtNCED3

To probe the localization of cysteine residues with respect to the metal-binding sites of AtCCD1 and AtNCED3, comparative homology models of the enzymes were produced using SWISS MODEL (Schwede et al. 2003), based on the ACO crystal structure template (Kloer et al. 2005). Both models maintained the overall ACO fold (which consists of a seven-bladed β propeller with four histidines at the propeller axis) and accommodated coordination of the metal binding site through the $^{\epsilon}$N of the four conserved histidine residues. AtCCD1 has five cysteine residues in total, including Cys74, Cys332, Cys352, Cys407, and Cys495. Only one of these (Cys352) was found to be proximally located to the metal binding site (8.5 Å from the iron center, Table 1A and Fig. 4A) and might thus serve as the reducing agent in the

Table 1. Homology-model-based Cys-Cys sulfur atom distances and Cys sulfur atom – iron distances for AtCCD 1 (A) and AtNCED3 (B).

(A) AtCCD1.					
	Distance (Å)				
	S_{C74}	S_{C332}	S_{C352}	S_{C407}	S_{C495}
S_{C332}	41.3				
S_{C352}	30.7	11.4			
S_{C407}	15.1	32.8	23.3		
S_{C495}	20.5	34.8	25.2	27.8	
Fe	28.8	18.6	8.5	22.2	23.1
(B) AtNCED3.					
	Distance (Å)				
	S_{C191}	S_{C407}	S_{C409}	S_{C430}	S_{C548}
S_{C407}	38.7				
S_{C409}	34.1	7.7			
S_{C430}	34.6	6.3	3.1		
S_{C548}	20.1	27.9	24.3	23.2	
Fe	22.1	18.3	12.4	13.6	17.7

Fig. 4. Secondary and tertiary structure analyses of AtCCD1. (A) Homology model of AtCCD1 based on the ACO crystal structure (Protein Data Bank accession No. 2BIW), maintains iron coordination based on interactions with the $^{\epsilon}$N of four conserved histidine residues, including His222, His270, His336, and His523. Proximities of Cys352 and Cys332 are highlighted. (B) Amino acid sequence alignments of carotenoid cleavage enzymes. AtCCD1, PhCCD1, CsCCD, and AAZ22349 all cleave 9,10 and (9′,10′) double bonds of carotenoids and are from *Arabidopsis thaliana*, crocus, petunia, and *Zea mays* respectively; AtCCD3 and Vp14 from *A. thaliana* and *Z. mays*, respectively, both cleave the 11,12 double bond of 9-*cis* epoxycarotenoids; ACO is from from *Syneccocystis*; AtCCD7 is a 9,10 double bond carotenoid cleavage dioxygenase from *A. thaliana*; AtCCD8 is a 13,14 double bond carotenoid cleavage dioxygenase from *A. thaliana*.

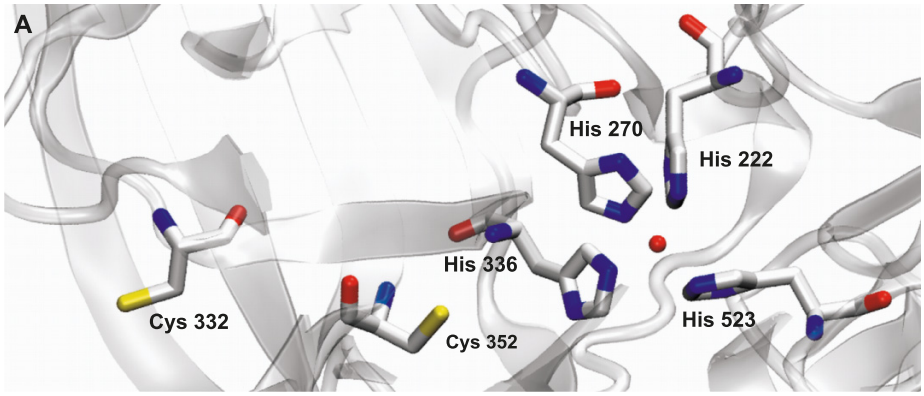

B

```
AtCCD1      NANAWEE-----EDEVVLITCRLENPDLDMVSGKV-------KEKLENFGN-ELYEMRFN 383
PhCCD1      NANAWEE-----GDEVVLITCRLPHPDLDMVNGEV-------KENLENFSN-ELYEMRFN 388
CsCCD       NANAWEE-----GDEVVLITCRLENPDLDMVNGAV-------KEKLENFKN-ELYEMRFN 387
AAZ22349    NANAWEE-----GDEVVLITCRLENPDLDKVNGYQ-------SDKLENFGN-ELYEMRFN 391
AtCCD3      LWNAWEEP----ETDEVVVIGSCMTP----PDSIF-------NESDENLKS-VLSEIRLN 455
Vp14        LWNAWEDE----ATGEVVVIGSCMTP----ADSIF-------NESDERLES-VLTEIRLD 456
CsZCD       VVNAWEEE----GGEVVVIVAPNVSP----IENAI-------DRFD-LLHV-SVEMARIE 220
ACO         HANAFEEN----GKIILDSICYNSLPQVDTDGDFR-------STNFDNLDPGQLWRFTID 353
AtCCD7      SGNAYETR----EDNGDLKIQIQASACSYRWFDFQ-------KMFGYDWQSNKLDPSVMN 447
AtCCD8      FINAYEEDKNGDGKATVIIADCCEHNADTRILDMLRLDTLRSSHGHDVLPDARIGRFRIP 432
```

formation of Cu^{+} in AtCCD1. Although distances between the different cysteine sulfur atoms in the model were all over 10 Å, precluding any obvious possible disulfides (Table 1A), closer scrutiny indicated that rotation of $\chi 1$ torsion angles for both Cys332 and Cys352 brings their sulfhydryl groups into significantly closer proximity, which, in the presence of an oxidizing Cu(II) in the metal binding pocket, might be sufficient to support disulfide formation, which does not otherwise occur. Further highlighting the localization of Cys332 is its position only 4 residues along the chain from His336, which coordinates metal in the active site. In contrast, AtNCED3 has six cysteine residues: Cys35, Cys191, Cys407, Cys409, Cys430, and Cys548, of which Cys35 could not be modeled because of its proximity to the N terminus, and none of the others was identified as being located within 10 Å of the iron-binding center

(Table 1B). As well, Cys430 and Cys409 are located in sufficiently close proximity to each other to putatively form a disulfide bond in the native structure.

Further, amino acid sequence alignment of select carotenoid cleavage enzymes indicates that Cys352 is conserved in AtCCD1 relatives (i.e., other enzymes known to cleave the 9,10 and 9′,10′ double bonds of carotenoids), but not in AtNCED3 or any other non-AtCCD1-like carotenoid cleavage enzymes (Fig. 4B). However, it should be noted that some of these other enzymes do maintain alternate cysteines localized in sequential proximity to the equivalent Cys352 position. Specifically, AtNCED3 Cys 430 is located two residues away along the amino acid chain from the equivalent AtCCD1 Cys352 position. Although this proximal sequential position might suggest that AtNCED3 Cys430 is equivalent to AtCCD1 Cys352, its more distal location from the iron site in the model ($\sim$14 Å), and its putative involvement in a native disulfide with Cys409 (which would preclude it from any role in reducing active site Cu(II)) argue against this. As well, AtNCED3 Cys409 is not conserved in AtCCD1 (see supplementary data[2]), thus eliminating the putative disulphide bonding partner in the latter enzyme. Overall these secondary and tertiary structural analyses emphasize the uniqueness and proximity of the AtCCD1 Cys352 residue to the catalytic site in AtCCD1 and AtCCD1-like relatives. This proximity, along with that of the more distally located Cys332, could accommodate the cysteine-related silencing of the EPR signal described above and position the residue such that it may uniquely modulate metal or substrate binding or the cleavage reaction.

Characterization of AtCCD1 C352A mutant

To directly test the role of Cys352 in the AtCCD1 active site, a site specific mutation to alanine was constructed and the mutant protein was overexpressed and purified from *E. coli,* as described for the wild-type protein. UV/Vis spectra of the original C352A mutant, as well as EDTA- and Cu^{2+}-treated versions, were virtually identical to the corresponding spectra of the wild-type enzyme (Fig. 5A), precluding any role for the residue in the modulation of the different metal-binding affinity or steric accessibility constraints observed compared with AtNCED3. However, EPR analysis of Cu^{2+}-substituted C352A did yield a type II Cu EPR signal (Fig. 5B) with *g* and *A* values virtually identical to those of the Cu^{2+}-substituted AtNCED3 enzyme. These results indicate that Cys352 is indeed responsible for the EPR silence of Cu^{2+}-substituted wild-type AtCCD1, and supports the localized proximity of the residue to the catalytic site of the enzyme as identified in the homology model. This result also demonstrates that Cu^{2+} does substitute for Fe^{2+} in the active site of AtCCD1 despite the inability of EDTA to chelate the iron away from the enzyme. Related attempts to mutate cysteine residues in AtNCED3 led to irrecoverable aggregation of expressed protein (data not shown), making analysis impossible, but lending further emphasis to the possibility of a critical disulfide bond in this enzyme.

To further probe the role of Cys352 in AtCCD1, kinetic

Fig. 5. Spectral and enzymatic characterization of the AtCCD1 C352A mutant. (A) UV/Vis absorption spectrum of purified AtCCD1 C352A mutant showing characteristic iron bands. Line a, native protein; line b, protein treated with 50 mmol/L EDTA; line c, protein treated with 0.2 mmol/L $CuSO_4$. (B) Electron paramagnetic resonance spectrum of the Cu^{2+}-reconstituted AtCCD1 C352A mutant, acquired at 100 K, 9.3971 GHz, and 20 μW, with a modulation of l G (1 G = 0.1 mT). (C) Michaelis–Menten analyses of wild-type ATCCD1 (diamonds) and AtCCD1 C352A mutant (squares) reaction kinetics.

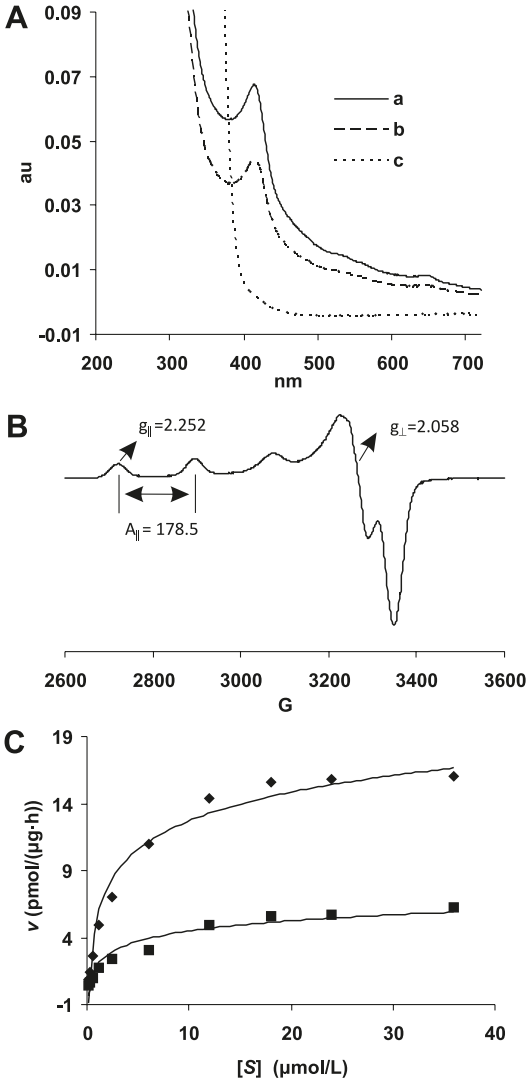

substrate cleavage analyses were carried out (Fig. 5C). The V_{max} of AtCCD1 (18.8 pmol/(μg protein·h)) was found to be about 2.6 times that of C352A (7.3 pmol/(μg protein·h)), whereas the K_m of AtCCD1 (3.5 μmol/L) was approximately 0.54 times that of C352A (6.24 μmol/L).

Overall, these results validate the homology model, which places Cys352 in proximity to the metal binding catalytic site in AtCCD1. The lack of a specific counterpart in AtNCED3, as suggested by both the homology model and

[2] Supplementary data for this article are available on the journal website (http://bcb.nrc.ca) or may be purchased from the Depository of Unpublished Data, Document Delivery, CISTI, National Research Council Canada, Building M-55, 1200 Montreal Road, Ottawa, ON K1A 0R6. DUD 3749. For more information on obtaining material, refer to http://cisti-icist.nrc-cnrc.gc.ca/cms/unpub_e.html.

sequence alignments, is supported by the lack of any corresponding EPR silencing effect. Thus, Cys352 represents a unique feature in proximity to the catalytic site of the AtCCD1 homologue and might account for observed differences in metal-binding affinities and (or) accessibilities or substrate binding and (or) cleavage specificities. In terms of assigning a mechanistic role to this uniquely localized cysteine, the UV/Vis absorption analyses of the C352A mutant showed that it maintains metal binding characteristics that are similar to those of wild-type AtCCD1. However, kinetic analyses demonstrated that Cys352 may play a role at the level of cleavage-related parameters, including substrate binding and reaction rates. Substrate binding and reaction rates have been determined for a variety of different carotenoid cleavage enzymes, including cowpea NCED3 (Han et al. 2004), maize VP14 (Schwartz et al. 2003), Mouse 15,15′ β-carotene cleavage enzymes (Paik et al. 2001; Poliakov et al. 2005), and cyanobacterial ACOs (Ruch et al. 2005; Scherzinger et al. 2006), yielding a broad spectrum of affinities and rates ranging from K_m values of 1.2 – 43 μmol/L and V_{max} values of 0.4–1200 pmol/(μg enzyme·h), depending on the enzymes, substrates, and reaction conditions. Assays of substrate cleavage for wild-type AtCCD1 and the associated C352A mutant gave rise to kinetic values that correlate with the mid-range reported reaction rates and substrate affinities of other carotenoid cleavage enzymes. Deletion of the reducing side chain specifically led to a decrease in V_{max} and an increase in K_m, thus highlighting the reduced substrate affinity and a slower rate of catalysis. Cysteine's role in substrate binding and catalysis could involve the maintenance of an optimally reduced state in the active site (as supported by the observed reduction of Cu^{2+} to Cu^{+}), or more simply, with creating specific steric substrate binding features or van der Waals contacts in the binding pocket. Experiments that further probe the significance of this residue in mediating the disparity in activities that exist between the different carotenoid cleavage enzymes are ongoing.

Acknowledgements

We thank Dr. J. Page, S. Polvi, and Dr. H. Chen (NRC/PBI) for help with HPLC, Dr. O.A. Kharenko for discussions and Dr. P.C. Loewen (University of Manitoba) for critical reading of the manuscript. We gratefully acknowledge the NRC Crops for Enhanced Human Health Program and the Saskatchewan Structural Sciences Centre for supporting this work. This manuscript has been assigned NRCC No. 48422.

References

Auldridge, M.E., McCarty, D.R., and Klee, H.J. 2006. Plant carotenoid cleavage oxygenases and their apocarotenoid products. Curr. Opin. Plant Biol. **9**: 315–321. doi:10.1016/j.pbi.2006.03.005. PMID:16616608.

Bouvier, F., Isner, J.C., Dogbo, O., and Camara, B. 2005. Oxidative tailoring of carotenoids: a prospect towards novel functions in plants. Trends Plant Sci. **10**: 187–194. doi:10.1016/j.tplants.2005.02.007. PMID:15817420.

Britton, G., and Young, A.J. 1993. Methods for the isolation and analysis of carotenoids. Chapman & Hill, London. pp. 409–459.

Coufal, D.E., Tavares, P., Pereira, A.S., Hyunh, B.H., and Lippard, S.J. 1999. Reactions of nitric oxide with the reduced non-heme diiron center of the soluble methane monooxygenase hydroxylase. Biochemistry, **38**: 4504–4513. doi:10.1021/bi9823378. PMID:10194372.

Coulter, E.D., Moon, N., Batie, C.J., Dunham, W.R., and Ballou, D.P. 1999. Electron paramagnetic resonance measurements of the ferrous mononuclear site of phthalate dioxygenase substituted with alternate divalent metal ions: direct evidence for ligation of two histidines in the copper(II)-reconstituted protein. Biochemistry, **38**: 11062–11072. doi:10.1021/bi9904499. PMID:10460161.

Creighton, T.E. 1984. Disulfide bond formation in proteins. Academic Press Inc., pp. 305–329.

D'Autreaux, B., Tucker, N.P., Dixon, R., and Spiro, S. 2005. A non-haem iron centre in the transcription factor NorR senses nitric oxide. Nature, **437**: 769–772. doi:10.1038/nature03953. PMID:16193057.

Deligiannakis, Y., Boussac, A., Bottin, H., Perrier, V., Barzu, O., and Gilles, A.M. 1997. A new non-heme iron environment in *Paracoccus denitrificans* adenylate kinase studied by electron paramagnetic resonance and electron spin echo envelope modulation spectroscopy. Biochemistry, **36**: 9446–9452. doi:10.1021/bi970021e. PMID:9235989.

Fester, T., Hause, B., Schmidt, D., Halfmann, K., Schmidt, J., Wray, V., et al. 2002. Occurrence and localization of apocarotenoids in arbuscular mycorrhizal plant roots. Plant Cell Physiol. **43**: 256–265. doi:10.1093/pcp/pcf029. PMID:11917079.

Franco, R., Pereira, A.S., Tavares, P., Mangravita, A., Barber, M.J., Moura, I., and Ferreira, G.C. 2001. Substitution of murine ferrochelatase glutamate-287 with glutamine or alanine leads to porphyrin substrate-bound variants. Biochem. J. **356**: 217–222. doi:10.1042/0264-6021:3560217. PMID:11336654.

Guex, N., and Peitsch, M.C. 1997. SWISS-MODEL and the Swiss-PdbViewer: an environment for comparative protein modeling. Electrophoresis, **18**: 2714–2723. doi:10.1002/elps.1150181505. PMID:9504803.

Han, S.Y., Kitahata, N., Sekimata, K., Saito, T., Kobayashi, M., Nakashima, K., et al. 2004. A novel inhibitor of 9-*cis*-epoxycarotenoid dioxygenase in abscisic acid biosynthesis in higher plants. Plant Physiol. **135**: 1574–1582. doi:10.1104/pp.104.039511. PMID:15247398.

Hegg, E.L., and Que, L., Jr. 1997. The 2-His-1-carboxylate facial triad–an emerging structural motif in mononuclear non-heme iron(II) enzymes. Eur. J. Biochem. **250**: 625–629. doi:10.1111/j.1432-1033.1997.t01-1-00625.x. PMID:9461283.

Hegg, E.L., Whiting, A.K., Saari, R.E., McCracken, J., Hausinger, R.P., and Que, L., Jr. 1999. Herbicide-degrading alpha-keto acid-dependent enzyme TfdA: metal coordination environment and mechanistic insights. Biochemistry, **38**: 16714–16726. doi:10.1021/bi991796l. PMID:10600135.

Hinks, J.A., Evans, M.C., De Miguel, Y., Sartori, A.A., Jiricny, J., and Pearl, L.H. 2002. An iron-sulfur cluster in the family 4 uracil-DNA glycosylases. J. Biol. Chem. **277**: 16936–16940. doi:10.1074/jbc.M200668200. PMID:11877410.

Hogan, D.A., Smith, S.R., Saari, E.A., McCracken, J., and Hausinger, R.P. 2000. Site-directed mutagenesis of 2,4-dichlorophenoxyacetic acidalpha-ketoglutarate dioxygenase. Identification of residues involved in metallocenter formation and substrate binding. J. Biol. Chem. **275**: 12400–12409. doi:10.1074/jbc.275.17.12400. PMID:10777523.

Humphrey, W., Dalke, A., and Schulten, K. 1996. VMD: visual molecular dynamics. J. Mol. Graph. **14**: 27–33.

Iuchi, S., Kobayashi, M., Taji, T., Naramoto, M., Seki, M., Kato, T., et al. 2001. Regulation of drought tolerance by gene manipulation of 9-*cis*-epoxycarotenoid dioxygenase, a key enzyme in

abscisic acid biosynthesis in Arabidopsis. Plant J. **27**: 325–333. doi:10.1046/j.1365-313x.2001.01096.x. PMID:11532178.

Kimura, S., Kikuchi, A., Senda, T., Shiro, Y., and Fukuda, M. 2005. Tolerance of the Rieske-type [2Fe-2S] cluster in recombinant ferredoxin BphA3 from *Pseudomonas* sp. KKS102 to histidine ligand mutations. Biochem. J. **388**: 869–878. doi:10.1042/BJ20042077. PMID:15733056.

Kloer, D.P., Ruch, S., Al-Babili, S., Beyer, P., and Schulz, G.E. 2005. The structure of a retinal-forming carotenoid oxygenase. Science, **308**: 267–269. doi:10.1126/science.1108965. PMID:15821095.

Kosman, D.J., Hassett, R., Yuan, D.S., and McCracken, J. 1998. Spectroscopic characterization of the Cu (II) sites in the Fet3 protein, the multinuclear copper oxidase from yeast required for high-affinity iron uptake. J. Am. Chem. Soc. **120**: 4037–4038. doi:10.1021/ja974104u.

Mathe, C., Mattioli, T.A., Horner, O., Lombard, M., Latour, J.M., Fontecave, M., and Niviere, V. 2002. Identification of iron(III) peroxo species in the active site of the superoxide reductase SOR from *Desulfoarculus baarsii*. J. Am. Chem. Soc. **124**: 4966–4967. doi:10.1021/ja025707v. PMID:11982354.

Mathieu, S., Terrier, N., Procureur, J., Bigey, F., and Gunata, Z. 2005. A carotenoid cleavage dioxygenase from *Vitis vinifera* L.: functional characterization and expression during grape berry development in relation to C13-norisoprenoid accumulation. J. Exp. Bot. **56**: 2721–2731. doi:10.1093/jxb/eri265. PMID:16131507.

Moise, A.R., von Lintig, J., and Palczewski, K. 2005. Related enzymes solve evolutionarily recurrent problems in the metabolism of carotenoids. Trends Plant Sci. **10**: 178–186. doi:10.1016/j.tplants.2005.02.006. PMID:15817419.

Notredame, C., Higgins, D.G., and Heringa, J. 2000. T-Coffee: A novel method for fast and accurate multiple sequence alignment. J. Mol. Biol. **302**: 205–217. doi:10.1006/jmbi.2000.4042. PMID:10964570.

Paik, J., During, A., Harrison, E.H., Mendelsohn, C.L., Lai, K., and Blaner, W.S. 2001. Expression and characterization of a murine enzyme able to cleave beta-carotene. The formation of retinoids. J. Biol. Chem. **276**: 32160–32168. doi:10.1074/jbc.M010086200. PMID:11418584.

Parry, A.D., and Horgan, R. 1991. Carotenoid metabolism and the biosynthesis of abscisic acid. Phytochemistry, **30**: 815–821. doi:10.1016/0031-9422(91)85258-2.

Poliakov, E., Gentleman, S., Cunningham, F.X., Jr., Miller-Ihli, N.J., and Redmond, T.M. 2005. Key role of conserved histidines in recombinant mouse beta-carotene 15,15'-monooxygenase-1 activity. J. Biol. Chem. **280**: 29217–29223. doi:10.1074/jbc.M500409200. PMID:15951442.

Rocklin, A.M., Tierney, D.L., Kofman, V., Brunhuber, N.M., Hoffman, B.M., Christoffersen, R.E., et al. 1999. Role of the nonheme Fe(II) center in the biosynthesis of the plant hormone ethylene. Proc. Natl. Acad. Sci. U.S.A. **96**: 7905–7909. doi:10.1073/pnas.96.14.7905. PMID:10393920.

Rocklin, A.M., Kato, K., Liu, H.W., Que, L., Jr., and Lipscomb, J.D. 2004. Mechanistic studies of 1-aminocyclopropane-1-carboxylic acid oxidase: single turnover reaction. J. Biol. Inorg. Chem. **9**: 171–182. doi:10.1007/s00775-003-0510-3. PMID:14714198.

Ruch, S., Beyer, P., Ernst, H., and Al-Babili, S. 2005. Retinal biosynthesis in Eubacteria: in vitro characterization of a novel carotenoid oxygenase from Synechocystis sp. PCC 6803. Mol. Microbiol. **55**: 1015–1024. doi:10.1111/j.1365-2958.2004.04460.x. PMID:15686550.

Ryle, M.J., and Hausinger, R.P. 2002. Non-heme iron oxygenases. Curr. Opin. Chem. Biol. **6**: 193–201. doi:10.1016/S1367-5931(02)00302-2. PMID:12039004.

Scherzinger, D., Ruch, S., Kloer, D.P., Wilde, A., and Al-Babili, S. 2006. Retinal is formed from apo-carotenoids in Nostoc sp. PCC7120: in vitro characterization of an apo-carotenoid oxygenase. Biochem. J. **398**: 361–369. doi:10.1042/BJ20060592. PMID:16759173.

Schmidt, H., Kurtzer, R., Eisenreich, W., and Schwab, W. 2006. The carotenase AtCCD1 from Arabidopsis thaliana is a dioxygenase. J. Biol. Chem. **281**: 9845–9851. doi:10.1074/jbc.M511668200. PMID:16459333.

Schwartz, S.H., Tan, B.C., Gage, D.A., Zeevaart, J.A., and McCarty, D.R. 1997. Specific oxidative cleavage of carotenoids by VP14 of maize. Science, **276**: 1872–1874. doi:10.1126/science.276.5320.1872. PMID:9188535.

Schwartz, S.H., Qin, X., and Zeevaart, J.A. 2001. Characterization of a novel carotenoid cleavage dioxygenase from plants. J. Biol. Chem. **276**: 25208–25211. doi:10.1074/jbc.M102146200. PMID:11316814.

Schwartz, S.H., Tan, B.C., McCarty, D.R., Welch, W., and Zeevaart, J.A. 2003. Substrate specificity and kinetics for VP14, a carotenoid cleavage dioxygenase in the ABA biosynthetic pathway. Biochim. Biophys. Acta, **1619**: 9–14. PMID:12495810.

Schwede, T., Kopp, J., Guex, N., and Peitsch, M.C. 2003. SWISS-MODEL: An automated protein homology-modeling server. Nucleic Acids Res. **31**: 3381–3385. doi:10.1093/nar/gkg520. PMID:12824332.

Smith, D.B., and Johnson, K.S. 1988. Single-step purification of polypeptides expressed in *Escherichia coli* as fusions with glutathione-*S*-transferase. Gene, **67**: 31–40. doi:10.1016/0378-1119(88)90005-4. PMID:3047011.

Solomon, E.I. 2001. Invited award contribution for ACS Award in Inorganic Chemistry. Geometric and electronic structure contributions to function in bioinorganic chemistry: active sites in non-heme iron enzymes. Inorg. Chem. **40**: 3656–3669. doi:10.1021/ic010348a. PMID:11442362.

Tan, B.C., Joseph, L.M., Deng, W.T., Liu, L., Li, Q.B., Cline, K., and McCarty, D.R. 2003. Molecular characterization of the *Arabidopsis* 9-*cis* epoxycarotenoid dioxygenase gene family. Plant J. **35**: 44–56. doi:10.1046/j.1365-313X.2003.01786.x. PMID:12834401.

Tocheva, E.I., Rosell, F.I., Mauk, A.G., and Murphy, M.E. 2004. Side-on copper-nitrosyl coordination by nitrite reductase. Science, **304**: 867–870. doi:10.1126/science.1095109. PMID:15131305.

Whiting, A.K., Que, L., Jr., Saari, R.E., Hausinger, R.P., Fredrick, M.A., and McCracken, J. 1997. Metal coordination environment of a Cu(II)-substituted α -keto acid-dependent dioxygenase that degrades the herbicide 2,4-D. J. Am. Chem. Soc. **119**: 3413–3414. doi:10.1021/ja964449x.

Wolz, E., Liechti, H., Notter, B., Oesterhelt, G., and Kistler, A. 1999. Characterization of metabolites of astaxanthin in primary cultures of rat hepatocytes. Drug Metab. Dispos. **27**: 456–462. PMID:10101140.